Chemistry–A European Journal
Research Article
doi.org/10.1002/chem.202501735
Chemistry Europe
European Chemical Societies Publishing
www.chemeurj.org

VIP *Very Important Paper*

Fluorine-Directed Structure-Specific Carbon Nanothreads

Guangwei Che,[a] Xingyu Tang,[a] Puyi Lang,[a] Jie Liu,[a] Yajie Wang,[a] Xuan Wang,[a] Xiaoge Wang,[b] Jing Ju,[b] Aijiao Guan,[c] Qian Li,[c] Junfeng Xiang,[c] Lutong Guo,[c] Yali Qiao,[c] Xiao Dong,[d] Ho-kwang Mao,[a] Haiyan Zheng,[a] and Kuo Li*[a]

Carbon nanothread (CNTh) is a sp^3-bonded one-dimensional nanomaterial that was predicted to combine the extreme strength with excellent flexibility. However, the reported CNTh usually has a nonuniform intrathread structure, and the synthesis of structure-specific CNTh is still a big challenge. Here, we selected 1,2,3-trifluorobenzene (1,2,3-TFB) with strong dipole as a precursor. By compressing 1,2,3-TFB to 20.1 GPa, a CNTh with a "zipper polymer" structure is obtained. Under applied pressure, 1,2,3-TFB are anti-parallelly stacked in column, and polymerize via selective sequential [4 + 2] polymerization between H-carbon dienophile/F-carbon dienophile and F, H-carbon diene within the column, followed by the "zippered" bonding of the rest atoms. The obtained CNTh is highly hydrophobic with contact angle of 124.6°. The excellent columnar anti-parallel $\pi\cdots\pi$ stacking and distinct reactivities of carbon atoms introduced by the F-substitution are responsible for the high reaction selectivity, which provides new insight for the precise synthesis of atom-level ordered CNThs.

1. Introduction

Starting from organic molecules, bottom-up synthesis brings many new members to the family of carbon materials, and novel carbon-based materials with atomic precision is therefore expected. Carbon nanothread (CNTh) is a novel one-dimensional (1 D) diamond-like material that is predicted to have extremely high strength (26.4 nN), stiffness (850 GPa), tenacity (4.1×10^7 N·m/kg), and diverse applications like sensor, energy storage, and nanoelectromechanical device.[1–3] More than 50 basic structure models of CNThs based on the pressure-induced polymerization (PIP) of benzene were theoretically proposed, like tube (3,0), polymer-I, polytwistane, and zipper polymer, et al.,[4,5] and their properties are closely related to the intrathread structures. For example, tube (3,0) was predicted to have a band gap of 3.93 eV and high stiffness of 1.78 TPa,[6,7] compared with 8.1 eV and 625.26 GPa of polytwistane.[8] Experimentally, CNTh was first synthesized by compression of benzene.[9,10] Suffering from the T-shape stacking and similar reactivity of the six aromatic carbon atoms, numbers of bonding pathways like [4 + 2] cycloaddition and *para*-polymerization compete in the polymerization process, and generate various connections.[11] Introducing heteroatoms and effective $\pi\cdots\pi$ stacking of monomers can improve the intrathread and interthread ordering of CNThs. Recently, several aromatics including furan,[12] thiophene,[13] and pyridazine[14] were reported to polymerize into CNThs under high-pressure via unique [4 + 2] cycloaddition, in obvious contrast to the multiple competing reaction pathways in benzene. However, the interunit bonds are typically limited to two, like ladder polymers, and degraded their strength and stiffness, etc., comparing to pure-carbon CNTh.[15] On the other hand, arene and perfluoroarene can form a sandwich-like stacking, which leads to pure-carbon skeletal CNThs with good interthread ordering. However, the intrathread structure is still controversial due to the similar reactivity of the carbon atoms in perfluoroarene / arene molecules, as discussed in the literature.[16–18] The synthesis of CNTh with specific intrathread structure from aromatic hydrocarbons is still very challenging.

1,2,3-Trifluorobenzene (1,2,3-TFB), in contrast to the perfluoroarene discussed above, is a polar molecule with partial fluorination. Under external pressure, 1,2,3-TFB crystallizes in a monoclinic lattice with space group *C*2/*c* as shown in Figure 1a. The molecules are anti-parallelly stacked in columns along *c*-axis, with the molecular plane approximately perpendicular to the *c*-axis, which provides an excellent geometry for the preparation of ordered CNTh. In this paper, we synthesized a structure-specific "zipper polymer" CNTh by compressing 1,2,3-TFB to 20.1 GPa. The strong dipole and anti-parallelly columnar stacking promoted the sequential [4 + 2] reaction between specific carbon atoms, and therefore improved the ordering of the CNTh. The obtained F-modified CNTh is highly hydrophobic with contact angle of 124.6°. Our work reported an all-carbon skeleton CNTh with a specific structure, and highlighted the fact that the partial F-substitution can

[a] G. Che, X. Tang, P. Lang, J. Liu, Y. Wang, X. Wang, H.-kwang Mao, H. Zheng, Dr. K. Li
Center for High Pressure Science and Technology Advanced Research, Beijing, China
E-mail: likuo@hpstar.ac.cn

[b] X. Wang, J. Ju
College of Chemistry and Molecular Engineering, Peking University, Beijing, China

[c] A. Guan, Q. Li, J. Xiang, L. Guo, Y. Qiao
Institute of Chemistry, Chinese Academy of Science, Beijing, China

[d] X. Dong
Key Laboratory of Weak-Light Nonlinear Photonics, School of Physics, Nankai University, Tianjin, China

Supporting information for this article is available on the WWW under https://doi.org/10.1002/chem.202501735

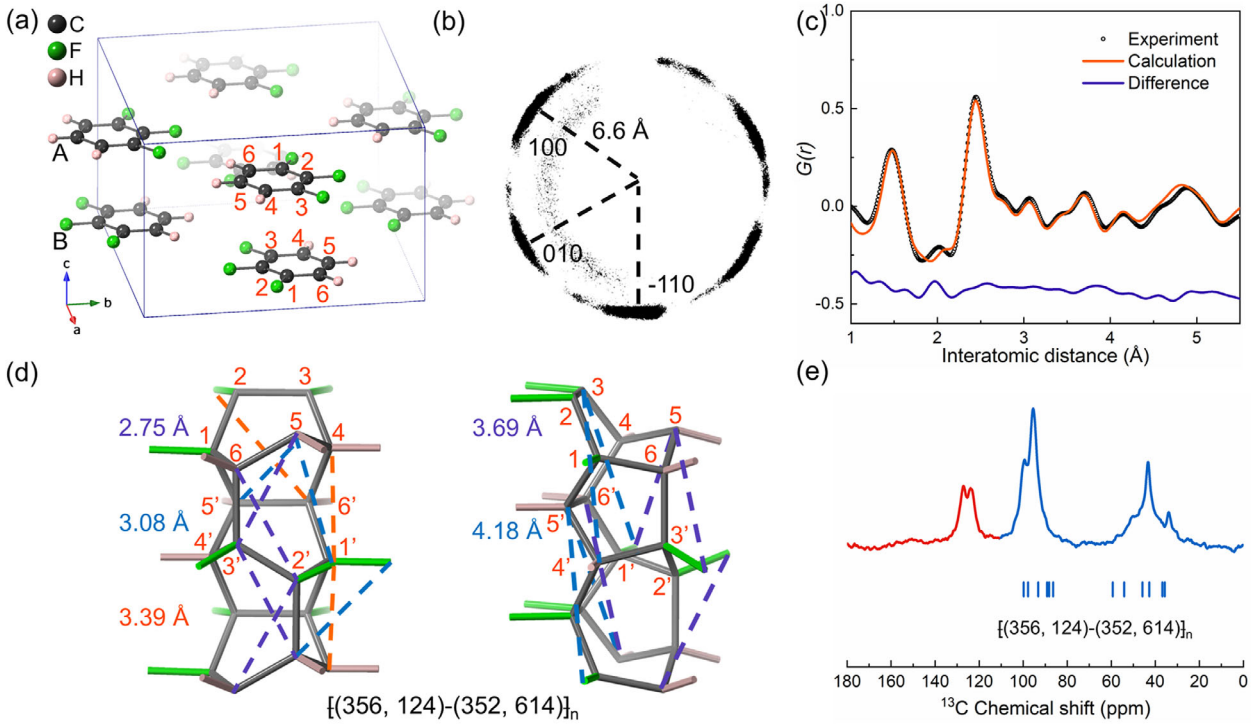

Figure 1. Structural investigations of PE-30. a) Crystal structure of the monomer 1,2,3-TFB at 1.4 GPa. The carbon atoms are numbered from 1 to 3 (-F) and 4 to 6 (-H) clockwise. b) The 2D XRD pattern of PE-30. The top diffraction pattern was partially covered by beam stoper. c) X-ray PDF refinement plot of PE-30 using the (356, 124)-(352, 614)$_n$ model with R_w = 0.186. d) The distance of atom-pairs and the assignment to the peaks in *G(r)* pattern. e) ^{1}H-^{13}C CP ssNMR with ^{1}H decoupling of PE-30 and the simulated chemical shifts of (356, 124)-(352, 614)$_n$ CNTh (blue vertical bars).

direct the reaction pathway in the high-pressure synthesis of carbon-materials.

2. Results and Discussion

2.1. Synthesis and structure of CNThs

We first loaded transparent liquid 1,2,3-TFB into a DAC cryogenically in liquid nitrogen bath and compressed it up to 39.9 GPa. After decompression, a white solid product was obtained. The product shows a hexagonal symmetry in the 2D XRD pattern with *d*-spacing of 6.6 Å, which is indexed by a 2D lattice (*a**-*b**) as shown in Figure 1b. This *d*-spacing represents the interplanar distance between the layers formed by parallelly stacked CNThs (Figure S1), which is a typical feature of CNThs synthesized by the PIP of aromatic molecules, etc.,[9,19] and indicates that the products are CNThs with hexagonal preferred orientation on *a*-*b* plane.

The ordering on the *c*-axis is often disturbed by the random shift between the threads along their axis,[9,20] so we have to employ total scattering and spectroscopic methods to investigate the intrathread structure. We synthesized milligrams of the solid product at 30 GPa using Paris-Edinburgh press (PE-30). PE-30 is identical to the product recovered from 40.1 GPa in DAC, as their IR spectra are the same, and the main peak of 1,2,3-TFB around 1500 cm^{-1} disappeared, indicating no reactant is left in PE-30 (Figure S2).

We performed X-ray Pair distribution function (PDF), ^{13}C cross-polarization (CP) ssNMR with ^{1}H decoupling, and Gas Chromatography-Mass Spectrometry (GC-MS) experiments on PE-30. X-ray PDF describes the distribution of distances between atomic pairs and is therefore a powerful tool to give the local structure of CNTh. The previously proposed models, including tube (3,0), polymer-I, polytwistane, and zipper polymer, are investigated as candidates (Figure S3). To name the models systematically, we use the numbers in 1,2,3-TFB to describe the bonding in the models. As shown in Figure 1a, the C atoms that bond to F are numbered as C1, 2, and 3, following a clockwise order in the lattice, and those bonded to H are C4, 5, and 6 (although C1 and C3, C4 and C6, as well as several other H and F atoms are crystallographically identical, we need to number them separately for the subsequent discussion). Taking zipper polymer as an example (Figure S3), both of the two isomers (356, 124)-(352, 614)$_n$ (the C1, 2, and 4 of the first molecule bonding to C3, 5, and 2 of the second molecule, respectively, and the C6, 1, and 4 of the second molecule bonding to the C3, 5, and 6 of the first molecule in the next repeating unit) and (256, 134)-(362, 514)$_n$ were considered.

By performing the PDF refinement as shown in Figure 1c, we found that only the (356, 124)-(352, 614)$_n$ well fits the experimental data. The first peak at 1.47 Å is ascribed to the overlap of the nearest-neighbor C-C pair and C-F pair, which demonstrates the presence of the sp^3-carbon. The peak at r = 2.43 Å corresponds to the distance between a sp^3-carbon and its next neighbor carbon in a six-membered ring and is common in almost all the models. The difference starts from the shoulder

at 2.75 Å. This is attributed to the distance between a sp^3-carbon and its next-neighbor carbon in a seven-membered ring (Figure 1d), which does not overlap with the peak at 2.43 Å due to the strain in the seven-membered ring. Among the models, only the zipper polymer contains a seven-membered ring (five-, six-, and seven-membered rings), while tube (3,0), and polytwistane only contains six-membered rings, and polymer-I contains five, five- and eight-membered rings. This is important evidence that demonstrates the zipper polymer. Beyond that, the peaks at r = 3.08, 3.39, 3.69, and 4.18 Å correspond to the distance between C5-C5′, F2-C6′, C5-F1′, and C3-F1′ in the (356, 124)-(352, 614)$_n$, respectively (Figure 1d). In contrast, others models, even for the other zipper polymer (256, 134)-(362, 514)$_n$, have obvious difference that can not be neglected in the fitting, and are therefore excluded, as shown in Figure S4.

The ^{1}H-^{13}C CP ssNMR with ^{1}H decoupling of PE-30 disclosed three types of carbon atoms as shown in Figure 1e. The peak centered at 34 and 43 ppm corresponds to C(sp^3) with hydrogen atoms (H-CR_3). This was clearly demonstrated by ^{1}H-^{13}C CP ssNMR with short, one-bond cross-polarization from ^{1}H to ^{13}C (contact time = 50 μs)[21,22] as shown in Figure S5. The peaks at 96 and 99 ppm are assigned to C(sp^3) bonded to fluorine (F-CR_3), which is demonstrated by the ^{19}F-^{13}C CP ssNMR with same short contact time of 50 μs at different excitation frequencies of -135 and -197 ppm, respectively, as shown in Figure S6. The signals at 124 and 127 ppm are ascribed to H-C(sp^2), as demonstrated by ^{1}H-^{13}C CP ssNMR with short contact time (contact time = 50 μs, Figure S5), which are contributed by some unreacted carbon atoms. In contrast, F-C(sp^2) undergoes a complete transition, indicating its higher reactivity. The simulated ^{13}C ssNMR (blue bars in Figure 1e) of (356, 124)-(352, 614)$_n$ is consistent with the experimental results, especially in the positions of the main peaks, which again evidenced the (356, 124)-(352, 614)$_n$ model.

GC-MS was also employed to investigate the reaction routes. PE-30 was extracted by *n*-hexane, and the oligomers in supernatant were analyzed by GC-MS. The components with abundance above 0.3% are compared to the reported oligomers of PIP product of C_6H_6-C_6F_6 cocrystal[23] and examined in the National Institute of Standards and Technology /Wiley standard library (Figure 2a and S7, S8). The identified oligomers can be summarized in two groups. The first group includes two dimers $C_{10}H_4F_4$, $C_{10}H_3F_5$, and a trimer $C_{18}H_9F_9$. The mass spectra of $C_{10}H_4F_4$ and $C_{10}H_3F_5$ show a strong molecular ion peak and similar fragmentation as naphthalene and therefore identified as F-substituted naphthalene. It was formed via [4 + 2] reaction and a following retro [4 + 2] reaction as well as elimination of the bridgehead H and/or F as shown in Figure 2b. $C_{18}H_9F_9$ is identified as a trimer formed by [4 + 2] reaction, as it fragmented into $C_6H_3F_3$ fragment via retro-Diels-Alder reaction in mass spectra (Figure S9a).[23] Therefore, the first group compounds are regarded as the featured oligomers via [4 + 2] reaction. The second group contains $C_{12}H_5F_5$, $C_{12}H_4F_6$, $C_{12}H_6F_4$, and $C_{18}H_7F_7$, with a common formula $C_{6n}(H, F)_{4n+2}$ (n = 2 and 3). They are identified as F-substituted biphenyls and terphenyls by comparing to the standard mass spectrum of $C_{12}H_2F_8$ and $C_{18}H_{14}$. These polyphenyls are from the 1,1′-coupling of 1,2,3-TFB, which was also proposed for the high-pressure reaction of aromatic molecules.[5,23]

As both the products of [4 + 2] and 1,1′-coupling reaction were observed in GC-MS, we then investigated their quantities to evaluate their contribution in the formation of CNTh. As shown in Figure 2a, the F-biphenyl has the highest content of 79.72% in sum. However, the content of F-terphenyl reduces to 3.95%. This indicates that the higher degree of polymerization via 1,1′-coupling was strongly suppressed. In contrast, $C_{10}H_4F_4$ (0.34%), $C_{10}H_3F_5$ (0.35%), and $C_{18}H_9F_9$ (0.85%) are the featured oligomers of [4 + 2] reaction. The abundance increases a little bit with degree of polymerization, which suggests that the PIP of 1,2,3-TFB follows [4 + 2] reaction to form CNTh.

Inspired by the GC-MS result, the MS with Direct-Exposure Probe (DEP-MS) of PE-30 was also measured to investigate the products with higher degree of polymerization. PE-30 was extracted by *n*-hexane, and the supernatant and suspension were examined by DEP-MS, respectively. The accumulated mass spectra of all products in supernatant from DEP-MS to GC-MS (Figure 2c) have similar intensity distribution, which demonstrates the composition of the supernatant in DEP-MS is the same as that in GC-MS. However, the abundance of $C_{18}H_9F_9$ ([4 + 2] route) in suspension is enhanced significantly, even higher than $C_{18}H_7F_7$ (1–1′ coupling) in quantity. This indicates the [4 + 2] products have a bigger abundance in the solid. Furthermore, the oligomers of higher degree of polymerization, $C_{6n}H_{3n}F_{3n}$ and $C_{6n}H_{2n+1}F_{2n+1}$ (n = 4, 5) in suspension were also detected by DEP-MS, and the ratio of $C_{6n}H_{3n}F_{3n}/C_{6n}H_{2n+1}F_{2n+1}$ increased with increasing degree of polymerization (Figure 2d). All these results confirmed that the [4 + 2] reaction predominates in the formation of CNTh.

In the above investigations, the PDF measurement disclosed the local connections within the CNTh, while the ssNMR experiment confirmed the local environment of the carbon atoms, and the MS results uncovered the two competing reaction routes from monomers to oligomers. It should be noted that the [4 + 2] reaction is related to the zipper polymer and polytwistane.[5] All these experimental results demonstrated that the 1,2,3-TFB undergoes [4 + 2] reaction to form the zipper polymer CNTh under external pressure.

2.2. High-pressure transformation process of 1,2,3-TFB

To track the reaction process, we investigated the in situ XRD of 1,2,3-TFB as shown in Figure 3a. At 1.4 GPa and room temperature, 1,2,3-TFB crystallized into the monoclinic phase with space group of *C*2/*c*, as determined by the Rietveld refinement (Figure S10, the atomic coordinates shown in Table S1). With increasing pressure up to 18.5 GPa, all the peaks slowly shift to high angle. The cell volumes as a function of pressure were fitted by using the third-order Birch–Murnaghan equation of state,[24] and two curves were used to fit the data (Figure S11a), indicating a minor phase transition at 4.8 GPa. This is also evidenced by Raman and IR results (Figure S12, Table S2 and S3). According to the Rietveld refinement results at higher pressure, we found

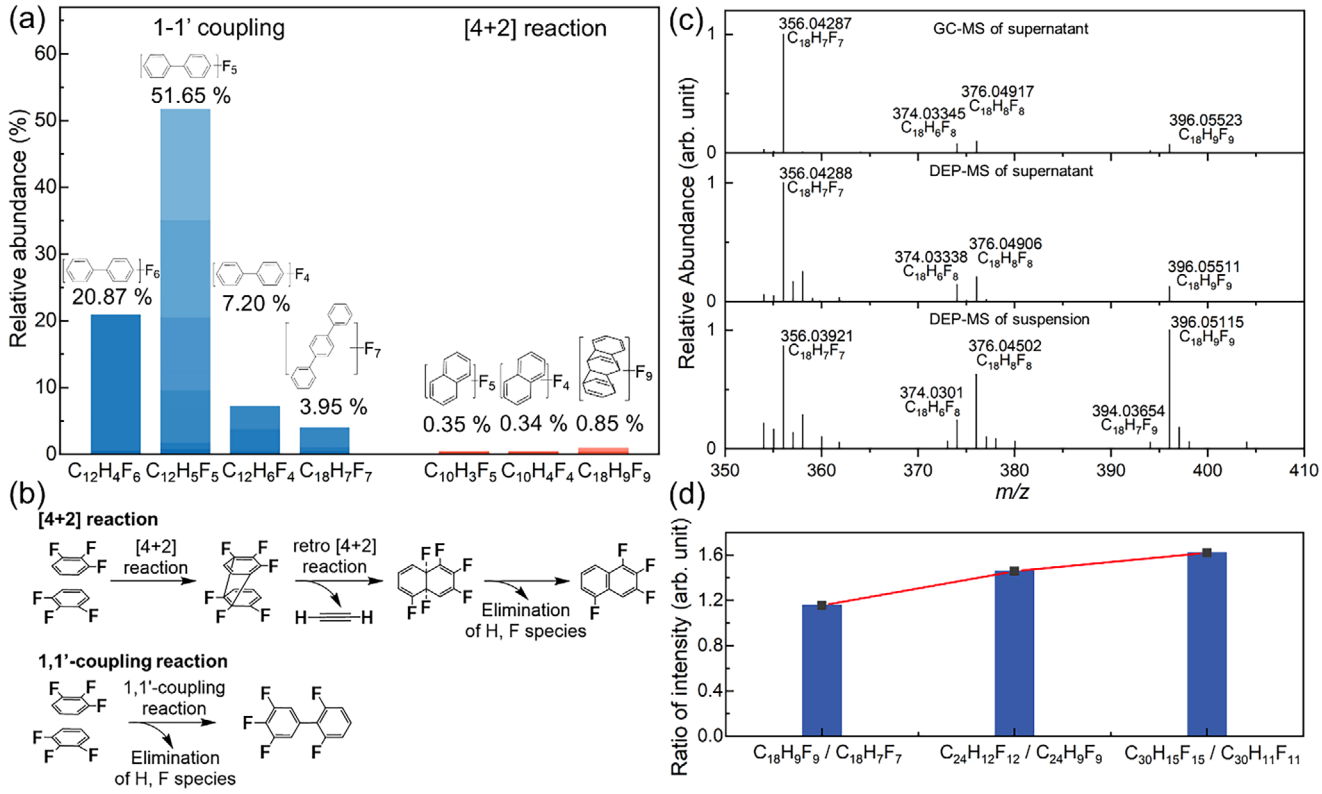

Figure 2. Mass-spectrum investigations of PE-30. a) Content of oligomers from [4 + 2] to 1,1′-coupling reactions in supernatant of PE-30 detected by GC-MS. Besides these two groups, the oligomer $C_{18}H_8F_8$ was also observed, which is the H, F-eliminated trimer, and likely results from sequential [4 + 2] reaction to 1,1′-coupling reaction (mass spectrum shown in Figure S9b). b) Proposed reaction paths of 1,2,3-TFB under high-pressure. c) Accumulated mass spectra of GC-MS of supernatant (top), DEP-MS of supernatant (middle), and DEP-MS of suspension (bottom). d) The ratio of fragment intensities between $C_{6n}H_{3n}F_{3n}$ and $C_{6n}H_{2n+1}F_{2n+1}$ (n = 3, 4, and 5) from the DEP-MS results of suspension.

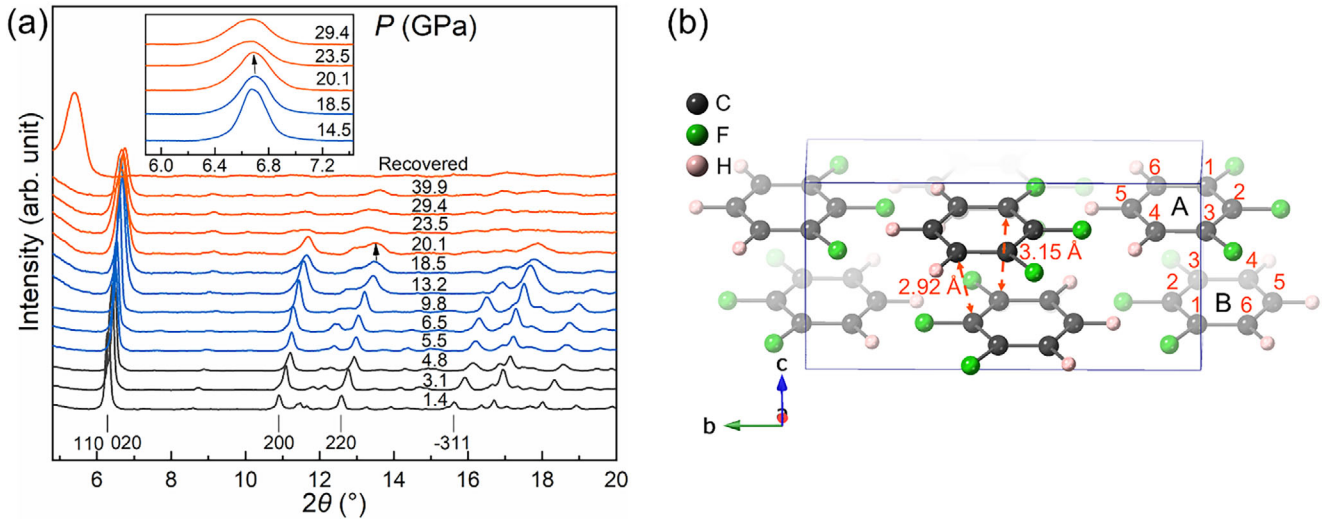

Figure 3. Crystallographic analysis of 1,2,3-TFB under high pressure. a) In situ XRD of 1,2,3-TFB under compression and decompression. b) Crystal structure of 1,2,3-TFB at threshold reaction pressure (18.5 GPa).

that this phase transition did not involve structural reconstruction. The evolution of lattice parameters from 1.4 to 16.7 GPa shows that the lattice is anisotropically compressed, with the *c*-axis ($\pi\cdots\pi$ stacking direction) having the maximum compression of 8% (Figure S11b). When pressure is increased up to 18.5 GPa, the peaks 110/020 (6.7°) and 220 (13.5°) shift to low angle. As the molecules are stacked along the *c*-axis, this indicates an expansion of inter-column *d*-spacing, which implies the onset of transformation from molecular column to thread. The polymerization is also confirmed by Raman and IR results (Figure S12). With pressure increasing up to 39.9 GPa, the peaks degraded with no new peak appearing, and only a broad peak of product

at 6.8° (d = 5.3 Å) maintained. When decompressed to ambient pressure, this peak shifts to 5.4° with the d-spacing of 6.6 Å.

The crystal structure of 1,2,3-TFB at the threshold pressure also supports the pathway of [4 + 2] reaction (Figure 3b). The cell parameters of 1,2,3-TFB at 18.5 GPa were determined by LeBail fitting (Figure S13), and the atomic coordinates were obtained by geometry optimization using DFT (Table S4). The 1,2,3-TFB molecules are still stacked along the c-axis, with the molecular plane approximately perpendicular to the c-axis. As the neighbor molecules in the column are shifted by $\frac{1}{2}$ c (correlated by the c-glide plane), the spaces and the local geometries between the stacked molecules are almost the same. Therefore, we can arbitrarily select a molecule A and its neighbor B for discussion of local geometry and reactions. The nearest intermolecular distances are 2.92 Å and 3.15 Å, between $C4_A$···$C2_B$ and $C1_A$···$C3_B$ (abbreviated as A41···B23), respectively. This is consistent with our conclusion again that the PIP of 1,2,3-TFB was initiated from [4 + 2] reaction, between B23 (dienophile) and A41(diene).

2.3. Mechanism of PIP of 1,2,3-TFB studied by theoretical calculation

To understand the reaction mechanism, the reaction path from the threshold structure to the (356, 124)-(352, 614)$_n$ was investigated by theoretical calculation using nudged elastic band (NEB) method at 20 GPa. The result is represented by blue curve in Figure 4a. Two energy barriers (marked as 1 and 3) were observed with a valley between them, suggesting an intermediate state. We performed geometry optimization from the intermediate 2, and a [4 + 2] polymer (56, 14)-(32, 14)$_n$ was obtained (configuration 5). Then we performed two NEB calculation: one from initial structure to the intermediate 5 and the other from intermediate 5 to product, with the result represented by the orange curve. The first step is the [4 + 2] reaction between B23 and A41, A56 and B14. The A6-B4 distance shrank significantly for bonding, with the B6-A3 distance almost unchanged (Figure 4a). The energy barrier is 52 kJ/mol per 1,2,3-TFB (configuration 4), forming the [4 + 2] polymer. The 52 kJ/mol includes the activation energy of forming two bonds upwards and two downwards, in average two bonds per molecule. This value is similar to the energy barrier of 2,2′-bipyrazine's [4 + 2] polymerization under high pressure,[25] which is low enough for the reaction to proceed at room temperature. Then the second step, zipper reaction of A2-B5 and B6-A3 occurred successively via an energy barrier of 2.6 kJ/mol per 1,2,3-TFB. The [4 + 2] reaction between B23 and A41 is also supported by the short C···C distances of 2.92 and 3.15 Å at threshold pressure (Figure 4a). Obviously, the [4 + 2] reaction is the crucial step in product formation, and the following "zipper" reaction only contains a slight movement of A23 and B56. The two steps are closely concerted, just like the forming of two bonds in cycloaddition reaction[12,13] and three bonds in the 1,3,5-concerted addition reaction (peri-cage reaction).[20]

As discussed above, the structure of product was determined as (356, 124)-(352, 614)$_n$ CNTh. As shown in Figure 4b, the [4 + 2] reaction path was demonstrated as the main path by combining with MS and theoretical calculations, and was supported by

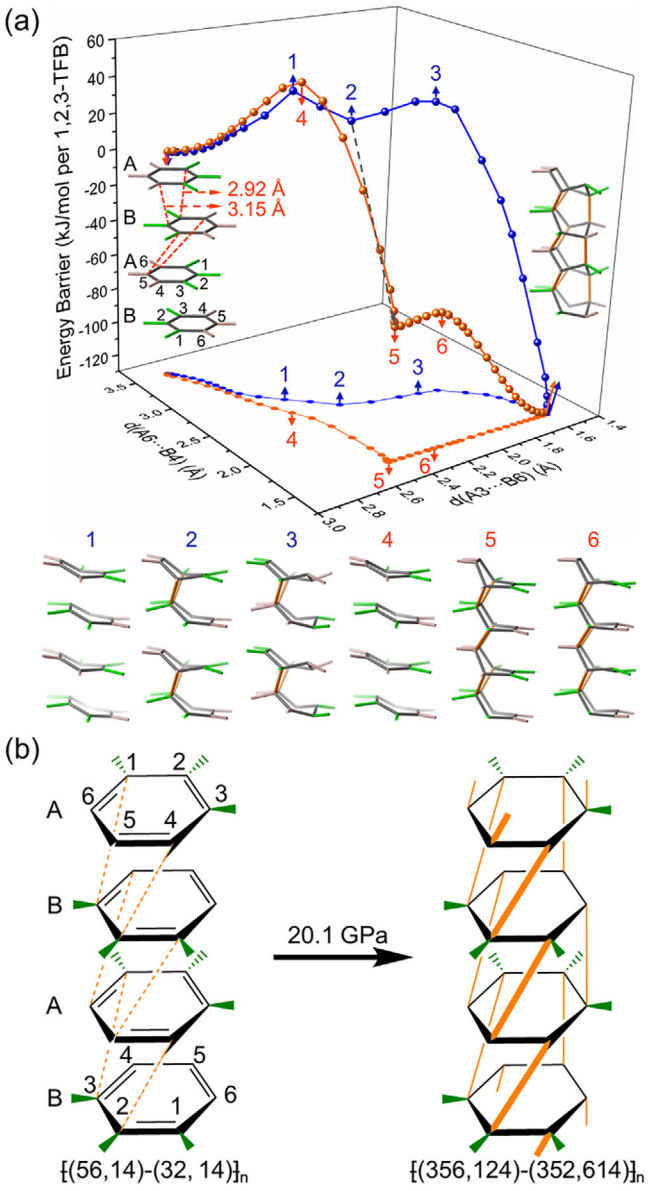

Figure 4. Reaction mechanism investigated by theoretical calculations. a) Enthalpy versus step curves. Blue and orange lines represent the computations before and after performing geometry optimization of the intermediate. The gray dotted line represents the geometry optimization from intermediate 2 to configuration 5. b) The [4 + 2] reaction pathway from 1,2,3-TFB to (356, 124)-(352, 614)$_n$ CNTh, with the newly formed bonds in orange.

in situ XRD result. This path was also in agreement with the theoretical report of Chen et. al.[5] Obviously the partial substitution of the fluorine atoms results in a strong dipole, which again results in the anti-parallel stacking and plays an important role to control the reaction pathway, and finally leads to the pure carbon-based nanothread with uniform chemical structure. In comparison, the heteroatoms were incorporated in the precursors when obtaining the structure-specific nanothreads $C_3N_3H_3$ tube (3,0) CNTh,[20] poly-pridazine,[14] and poly-furan.[12] Although the heteroatoms can direct the reaction pathway, less chemical bonding was formed due to its reactive inertness, which will affect the mechanical properties of the CNTh.

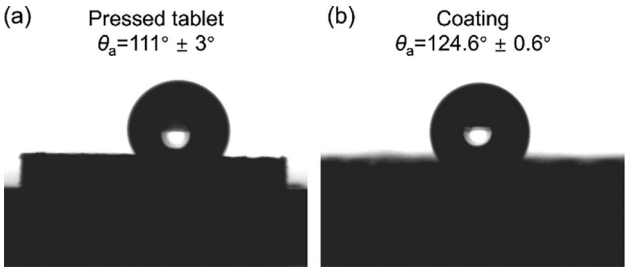

Figure 5. Hydrophobicity investigation of PE-30. Optical images of the contact angle on a) pressed PE-30 tablet and b) PE-30-coated silicon wafer. The uncertainty of the contact angle measurements is determined by three independent measurements at three different locations on one sample.

The even-distributed fluorine atoms also bring hydrophobicity to (356, 124)-(352, 614)$_n$ CNThs. To assess the intrinsic hydrophobic property of fluorine-modified CNThs, we prepared tablet of PE-30 with smooth surface as possible, and its water contact angle was measured as 111 ± 3° as shown in Figure 5a. We also prepared a stable dispersion of PE-30 in dimethylsulfoxide (DMSO) and coating the PE-30 on silicon wafer (Figure S14). The contact angle was 124.6 ± 0.6° as shown in Figure 5b. Comparing with the conventional polytetrafluoroethylene with contact angle of 113.8 ± 1.4°,[26] fluorine modified CNThs show excellent hydrophobic behavior with possible high strength, which may be used as high-strength hydrophobic fibers.

3. Conclusion

In conclusion, we experimentally demonstrated that 1,2,3-TFB experiences [4 + 2] reaction under high-pressure and form (356, 124)-(352, 614)$_n$ CNTh. The theoretical calculation also confirms the pathway of [4 + 2] reaction between B23 (dienophile) and A41(diene), A56 (dienophile) and B14 (diene), respectively. The subsequent zipper reaction happened with much lower energy barrier, and these two reaction steps can be even recognized as a concerted process. This high reaction selectivity and the obtained CNThs with uniform chemical structure are due to the partial substitution of the fluorine atoms. Furthermore, the F atoms also bring the hydrophobicity to the carbon materials and the F-modified CNThs was demonstrated to have similar hydrophobic property as polytetrafluoroethylene, with the contact angle at 124.6°, but high tensile strength can be expected due to its diamond-like local structures. Our research highlights that F-substitution is effective to generate specific structure CNTh by adjusting molecular arrangement and affecting the reactivity of C atoms. Our work also provides a designable solid-state synthesis method for functional CNTh with specific all-carbon skeleton, and more hydrophobic 1D diamond-based materials with high strength, stiffness, and tenacity can be expected.

4. Experimental Section

Synthesis of poly-1,2,3-trifluorobenzene carbon nanothreads (CNThs) by using a diamond anvil cell (DAC) under high-pressure and room-temperature: 1,2,3-trifluorobenzene (1,2,3-TFB, >98.0%, GC purity grade) was purchased from Aladdin and used without further purification. Symmetric DACs with the anvil culet of 300 μm in diameter were used to apply the high pressure. 1,2,3-TFB was loaded into the DAC cryogenically in liquid nitrogen and compressed to 40.1 GPa. A white transparent solid was obtained after decompression, and the reactant evaporated rapidly and completely, with the evidence from the IR spectra (Figure S2). T-301 stainless gaskets were pre-indented to 30 μm in thickness and center holes with d = 100 μm were drilled to serve as a sample chamber. The pressure of the sample was determined by the fluorescence peak of the ruby, according to the equation P (GPa) = 248.4[$(\lambda/\lambda_0)^{7.665}$–1].[27]

Synthesis of poly-1,2,3-trifluorobenzene CNThs by using a Paris-Edinburgh (PE) press under high-pressure and room-temperature: A VX3 PE press was used to synthesize the product of mg-scale. Double-toroidal sintered diamond anvils with 3 mm dimple diameters and encapsulated T301 stainless steel gaskets were used to generate the pressure. The PE press was driven by automatic hydraulic oil syringe pump, and the calibration curve from literature was used to estimate the pressure.[28] 1,2,3-TFB was loaded into the PE press cryogenically in liquid nitrogen, and the oil pressure was quickly increased to 150 bar (about 2.5 GPa on sample) to seal the sample. Then the sample was compressed to 30 GPa (oil pressure of 1400 bar) and kept at the desired pressure for about 12 hours. After releasing the pressure, 5 mg white powder was obtained when removing the gaskets. The unreacted 1,2,3-TFB was removed by volatilization at room temperature, which was evidenced by the IR spectra as shown in Figure S2.

Pair distribution function (PDF) measurement of PE-30: The synchrotron X-ray PDF experiment of the PE-30 was performed at 11-ID-B beamline of Advanced Photon Source (APS) at the Argonne National Laboratory (ANL). A polyimide capillary was used to load product (~10 mg). The incident X-ray was monochromated to 0.2115 Å. The CeO_2 standard sample was used to calibrate the Pilatus detector. Reducing the collected 2D data and subtracting the background of an empty capillary were performed by Dioptas software.[29] PDF getX3 software was used to reduce the *G(r)* data and the PDFgui2 software was employed for simulating and refining the PDF data of models.[30,31]

Solid-state nuclear magnetic resonance (ssNMR) measurement of PE-30: High-resolution ^{1}H-^{13}C cross-polarization (CP) magic angle spinning (MAS) with ^{1}H decoupling ssNMR experiment was performed on a Bruker NEO 600 MHz NMR spectrometer. A Bruker 1.3 mm MAS NMR probe with 1.3 mm ZrO_2 rotors was used. The contact time (CT) of cross-polarization is 4000 μs. The MAS frequency is 20 kHz. The spectrum was acquired with a recycling delay of 3 s, averaging 13 936 scans. The larmor frequency of ^{1}H and ^{13}C were 600.1 and 150.9 MHz. The methylene carbon of adamantane was used to calibrate the carbon chemical shifts at δ_C = 39 ppm.

High-resolution ^{1}H-^{13}C cross-polarization (CP) magic angle spinning (MAS) ssNMR experiment (Figure S5) was performed on a Bruker Avance III 600 MHz NMR spectrometer. A Bruker 1.3 mm MAS NMR probe with 1.3 mm ZrO_2 rotors was used. The MAS frequency is 20 kHz. The contact time of cross-polarization is 50 and 200 μs respectively. The spectrum was acquired with a recycling delay of 3 s, averaging 10 240 scans. The larmor frequency of ^{1}H and ^{13}C were 599.5 and 150.7 MHz. The methylene carbon of adamantane was used to calibrate the carbon chemical shifts at δC = 39 ppm.

High-resolution ^{19}F magic angle spinning (MAS) ssNMR experiment (Figure S6a) was performed on a Bruker NEO 600 MHz NMR

spectrometer. A Bruker 1.3 mm MAS NMR probe with 1.3 mm ZrO_2 rotors was used. The MAS frequency is 30 kHz. The Larmor frequency of ^{19}F was 564.6 MHz. The spectrum was acquired with a recycling delay of 6 s, averaging 40 scans. The fluoride of ammonium trifluoroacetate was used to calibrate the fluorine chemical shifts at δ_F = -74 ppm.

High-resolution ^{19}F-^{13}C cross-polarization (CP) magic angle spinning (MAS) ssNMR experiment (Figure S6b and S6c) was performed on a Bruker NEO 600 MHz NMR spectrometer. A Bruker 1.3 mm MAS NMR probe with 1.3 mm ZrO_2 rotors was used. The MAS frequency is 20 kHz. The contact time of cross-polarization was set as 50 and 2500 µs respectively. The spectrum was acquired with a recycling delay of 3 s, averaging 10 240 (Figure S6, CT = 2500 µs, excitation frequency = -135 ppm), 7400 (CT = 50 µs, excitation frequency = -135 ppm), 7888 (CT = 2500 µs, excitation frequency = -197 ppm), and 12 632 (CT = 50 µs, excitation frequency = -197 ppm) scans respectively. The methyl carbon of ammonium trifluoroacetate was used to calibrate the carbon chemical shifts at δ_C = 117 ppm.

High-resolution gas chromatography-mass spectrometry measurement (GC-MS) and direct exposure probe-mass spectrometry (DEP-MS) of PE-30: PE-30 was extracted by *n*-hexane (C_6H_{14}, chromatographical purity, >98.0%, Aladdin), and the supernatant was measured by GC-MS. High-resolution GC-MS measurement was performed on Thermo Scientific™ Q Exactive™ GC hybrid quadrupole-Orbitrap mass spectrometer. The oligomers in supernatant were separated by Thermo Scientific TRACETM 1310 GC with a TG-5SilMS capillary column (30 m × 0.25 mm inner diameter × 0.25 µm film thickness). Helium (99.999%) was used as a carrier gas with a constant flow rate of 1.0 mL/min. The 1 µL supernatant was injected manually with splitless mode at 280 °C. The temperature of GC oven was set from 40 °C (held for 2 minutes) to 280 °C (held for 10 minutes) at a rate of 5 °C/min. The temperature of the transfer lines was set at 280 °C. The Q Exactive Orbitrap system in mass spectrometer was tuned by an autotune procedure and calibrated by a calibration solution, for the target of the mass accuracy of < 1.0 ppm root mean square (RMS). The system was operated with an electron ionization source (EI) at 70 eV. The temperature of the ion source is 280 °C. The full scan mode at 60k resolving power (FWHM at *m/z* 200) mass resolution was used to record scan spectra in the range of 50–750 *m/z*.

For the Direct-Exposure Probe (DEP) experiment, PE-30 was also extracted by *n*-hexane (C_6H_{14}, chromatographical purity, >98.0%, Aladdin), then the supernatant and suspension of PE-30 were measured by DEP-MS, respectively. High-resolution DEP-MS measurements were performed on Thermo Scientific™ Q Exactive™ GC Orbitrap™ MS with Direct-Exposure Probe, which features a heating filament and is capable of flash vaporization or pyrolysis up to 2000 °C.

In situ high-pressure Raman, IR and X-ray diffraction experiments of 1,2,3-TFB: Symmetric DACs with the anvil culet of 300 µm in diameter were used for the in situ Raman, IR, and XRD experiments. For IR experiments, a pair of type II diamonds was used. T-301 stainless gaskets were pre-indented to 30 µm in thickness and a hole of 100 µm in diameter was drilled to serve as a sample chamber. The pressure of the sample system was determined by the fluorescence peak of the ruby, based on the equation P (GPa) = 248.4[$(\lambda/\lambda_0)^{7.665}$–1].[27] All sample loading procedures were conducted under low temperature using liquid nitrogen, then the sample was sealed quickly to avoid the possible formation of big grains or preferred orientation. No pressure medium was used in these experiments.

For the in situ Raman experiments, a commercial Renishaw Raman microscope (RM1000) was used to collect Raman spectra and the appropriate laser wavelength of 532 nm was selected for excitation. Before measurements, the system was calibrated by the silicon line.

For in situ IR experiments, Bruker VERTEX 70v with HYPERION 2,000 microscope was used. A Globar was used as a conventional source. We collected the spectra in a transmission mode in the range of 600–4000 cm^{-1} with a resolution of 2 cm^{-1}. The absorption of the diamond anvils with the same area was used as the background and the aperture was set as 40 × 40 μm^2.

In situ synchrotron X-ray diffraction data under high pressure were collected at 15U beamline of Shanghai Synchrotron Radiation Facility. The incident X-ray was monochromated to the wavelength of 0.6199 Å and the beam size was 2 × 3 μm^2. The CeO_2 standard sample was used to calibrate the Pilatus detector. The data was reduced by using the Dioptas software.[29] The crystal structures and atomic positions of 1,2,3-TFB were determined by Rietveld refinement using the Jana 2006 package.[32]

Density Functional Theory (DFT) calculations: Density functional theory[33] calculations were performed to investigate the critical structure of 1,2,3-TFB in Cambridge Sequential Total Energy Package (CASTEP) module[34] in Material Studio. The critical structure of 1,2,3-TFB at 18.5 GPa was optimized with a space group *C*2/*c* lattice (a = 6.43 Å, b = 10.78 Å, c = 5.82 Å, β = 108.793°) based on the in situ XRD experiments. The local density approximation (LDA) exchange correlation function by Ceperley and Alder, as parameterized by Perdew and Zunger (CA-PZ)[35] was used in generated on the fly (OTFG) norm-conserving pseudopotentials with an energy cutoff of 840 eV. The k-points solution was $2\pi \times 0.04$ A^{-1}. DFT-D correction forward by Ortmann, Bechstedt, and Schmidt was used to describe the noncovalent interaction in the system.[36]

The structures of proposed CNTh models were constructed following the topo-chemical rule, and then subsequently optimized with variable lattice parameters using the geometry optimization of the Forcite module and CASTEP module. The simulated chemical shielding constants of proposed CNTh model was also calculated by CASTEP.[37] LDA-CA-PZ with OTFG norm-conserving pseudopotentials was implemented, with an energy cutoff of 840 eV. The chemical shifts were calculated as:

$$\delta_{CNTh}^{calc} = \sigma_{ref}^{calc} - \sigma_{CNTh}^{calc} + \delta_{ref}^{exp}$$

where σ_{CNTh}^{calc} and σ_{ref}^{calc} are the calculated chemical shielding of CNTh model, and the reference compound (adamantane). The δ_{ref}^{exp} is the experimental chemical shift of adamantane (methylene carbon of adamantane at 38 ppm).

Raman and IR spectra were calculated using CASTEP in Material Studio based on the crystal structure of 1,2,3-TFB.[38] The assignment of the Raman and IR peaks was shown in Table S1 and S2. LDA-CA-PZ with norm-conserving pseudopotentials was implemented, with an energy cutoff of 840 eV.

Variable cell nudged elastic band (vc-NEB) calculations[39]: The calculations were performed in Vienna Ab-initio Simulation Package (VASP)[40] with USPEX[41] code. For density functional theory (DFT) single-point calculations,[33] the projector-augmented plane-wave (PAW) method was used with LDA exchange-correlation function. Plane wave basis with 560 eV energy cutoff was adopted, and k-points mesh was in a spacing of $2\pi \times 0.05$ A^{-1}. To take the noncovalent effects into consideration, DFT-D3(BJ) correction was used.

For reaction path searching, a series of intermediate structures (images) were constructed between the initial state (IS) and the final state (FS). The variable-image-number method was employed to distribute the images at relatively uniform intervals along the path. The IS was the optimized structure of 1,2,3-TFB crystal at 18.5 GPa, while the key intermediates and the FS were obtained by shortening the intermolecular distances with subsequent optimizations. All structures along the path were optimized considering both the gradient of potential energy surface (PES) and the elastic forces applied by neighboring images until the minimum energy path (MEP) was found.

Contact angle measurement of PE-30: The contact angle was measured using optical contact angle measuring and contour analysis systems (OCA 25, dataphysics). The water (2 μL) was drop casted on the pressed tablet of PE-30 and the silicon wafer coated with PE-30 and the measurement of contact angle was subsequently performed at ambient conditions.

Acknowledgments

The authors acknowledge the support of the National Key Research and Development Program of China (2023YFA1406200 and 2019YFA0708502). The authors acknowledge the support of the National Natural Science Foundation of China (Grant Nos.: 22022101). This work was carried out with the support of beamline of 15U at Shanghai Synchrotron Radiation Facility. The pair distribution function data were collected at the 11-ID-B beamline of the Advanced Photon Source at the Argonne National Laboratory and the 13HB beamline of the Shanghai Synchrotron Radiation Facility. This study was also partially supported by Synergetic Extreme Condition User Facility (SECUF).

Conflict of Interest

There are no conflicts to declare.

Data Availability Statement

The data that support the findings of this study are available in the supplementary material of this article.

Keywords: 1,2,3-trifluorobenzene · fluorinated carbon nanothread · high pressure · hydrophobic

[1] R. E. Roman; K. Kwan; S. W. Cranford, *Nano Lett.* **2015**, *15*, 1585.
[2] P. G. Demingos; A. R. Muniz, *Carbon* **2018**, *140*, 644.
[3] H. Zhan; G. Zhang; J. M. Bell; V. B. C. Tan; Y. Gu, *Nat. Commun.* **2020**, *11*, 1905.
[4] E. S. Xu; P. E. Lammert; V. H. Crespi, *Nano Lett.* **2015**, *15*, 5124.
[5] B. Chen; R. Hoffmann; N. W. Ashcroft; J. Badding; E. S. Xu; V. Crespi, *J. Am. Chem. Soc.* **2015**, *137*, 14373.
[6] M.-M. Chen; J. Xiao; C. Cao; D. Zhang; L.-L. Cui; X.-M. Xu; M.-Q. Long, *AIP Adv.* **2018**, *8*, 075107.
[7] D. Stojkovic; P. Zhang; V. H. Crespi, *Phys. Rev. Lett.* **2001**, *87*, 125502.
[8] A. V. Domnin; V. V. Porsev; R. A. Evarestov, *Comput. Mater. Sci.* **2022**, *214*, 111704.
[9] T. C. Fitzgibbons; M. Guthrie; E. S. Xu; V. H. Crespi; S. K. Davidowski; G. D. Cody; N. Alem; J. V. Badding, *Nat. Mater.* **2015**, *14*, 43.
[10] W. Zhao; J. Zhang; Z. Sun; G. Xiao; H. Zheng; K. Li; M.-R. Li; B Zou, *CCS Chem.* **2025**, https://doi.org/10.31635/ccschem.025.202405293.
[11] P. Duan; X. Li; T. Wang; B. Chen; S. J. Juhl; D. Koeplinger; V. H. Crespi; J. V. Badding; K. Schmidt-Rohr, *J. Am. Chem. Soc.* **2018**, *140*, 7658.
[12] S. Huss; S. Wu; B. Chen; T. Wang; M. C. Gerthoffer; D. J. Ryan; S. E. Smith; V. H. Crespi; J. V. Badding; E. Elacqua, *ACS Nano* **2021**, *15*, 4134.
[13] A. Biswas; M. D. Ward; T. Wang; L. Zhu; H.-T. Huang; J. V. Badding; V. H. Crespi; T. A. Strobel, *J. Phys. Chem. Lett.* **2019**, *10*, 7164.
[14] S. G. Dunning; L. Zhu; B. Chen; S. Chariton; V. B. Prakapenka; M. Somayazulu; T. A. Strobel, *J. Am. Chem. Soc.* **2022**, *144*, 2073.
[15] P. G. Demingos; A. R. Muniz, *J. Phys. Chem. C* **2019**, *123*, 3886.
[16] M. D. Ward; W. S. Tang; L. Zhu; D. Popov; G. D. Cody; T. A. Strobel, *Macromolecules* **2019**, *52*, 7557.
[17] A. Friedrich; I. E. Collings; K. F. Dziubek; S. Fanetti; K. Radacki; J. Ruiz-Fuertes; J. Pellicer-Porres; M. Hanfland; D. Sieh; R. Bini; S. J. Clark; T. B. Marder, *J. Am. Chem. Soc.* **2020**, *142*, 18907.
[18] M. C. Gerthoffer; S. Wu; B. Chen; T. Wang; S. Huss; S. M. Oburn; V. H. Crespi; J. V. Badding; E. Elacqua, *Chem. Sci.* **2020**, *11*, 11419.
[19] X. Li; M. Baldini; T. Wang; B. Chen; E. S. Xu; B. Vermilyea; V. H. Crespi; R. Hoffmann; J. J. Molaison; C. A. Tulk; M. Guthrie; S. Sinogeikin; J. V. Badding, *J. Am. Chem. Soc.* **2017**, *139*, 16343.
[20] D. Gao; X. Tang; J. Xu; X. Yang; P. Zhang; G. Che; Y. Wang; Y. Chen; X. Gao; X. Dong; H. Zheng; K. Li; H.-k. Mao, *Proc. Natl. Acad. Sci. USA* **2022**, *119*, e2201165119.
[21] B. S. Matsuura; S. Huss; Z. Zheng; S. Yuan; T. Wang; B. Chen; J. V. Badding; D. Trauner; E. Elacqua; A. C. T. Duin; V. H. Crespi; K. Schmidt-Rohr, *J. Am. Chem. Soc.* **2021**, *143*, 9529.
[22] Y. Fu; Y. Yao; A. C. Forse; J. Li; K. Mochizuki; J. R. Long; J. A. Reimer; G. D. Paëpe; X. Kong, *Nat. Commun.* **2023**, *14*, 2386.
[23] Y. Wang; X. Dong; X. Tang; H. Zheng; K. Li; X. Lin; L. Fang; G. Sun; X. Chen; L. Xie; C. L. Bull; N. P. Funnell; T. Hattori; A. Sano-Furukawa; J. Chen; D. K. Hensley; G. Cody; Y. Ren; H. H. Lee; H.-k. Mao, *Angew. Chem. Int. Ed.* **2019**, *58*, 1468.
[24] F. Birch, *J. Geophys. Res.* **1978**, *83*, 1257.
[25] F. Li; X. Tang; Y. Fei; J. Zhang; J. Liu; P. Lang; G. Che; Z. Zhao; Y. Zheng; Y. Fang; C. Li; D. Gao; X. Dong; T. Hattori; J. Abe; H.-k. Mao; H. Zheng; K Li, *J. Am. Chem. Soc.* **2025**, *147*, 14054.
[26] H. Kang; S. H. Lee; K. Kim, *PLoS One* **2023**, *18*, e0282352.
[27] H.-k. Mao; J. Xu; P. M. Bell, *J. Geophys. Res.* **1986**, *91*, 4673.
[28] T. Hattori; A. Sano-Furukawa; S. Machida; J. Abe; K. Funakoshi; H. Arima; N. Okazaki, *High Press. Res.* **2019**, *39*, 417–425.
[29] C. Prescher; V. B. Prakapenka, *High Press. Res.* **2015**, *35*, 223–230.
[30] P. Juhás; T. Davis; C. L. Farrow; S. J. L. Billinge, *J. Appl. Crystallogr.* **2013**, *46*, 560.
[31] C. L. Farrow; P. Juhas; J. W. Liu; D. Bryndin; E. S. Božin; J. Bloch; T. Proffen; S. J. L. Billinge, *J. Phys.: Condens. Matter* **2007**, *19*, 335219.
[32] V. Petříček; M. Dušek; L. Palatinus, *Z. Kristallogr.* **2014**, *229*, 345.
[33] R. O. Jones, *Rev. Mod. Phys.* **2015**, *87*, 897.
[34] S. J. Clark; M. D. Segall; C. J. Pickard; P. J. Hasnip; M. I. J. Probert; K. Refson; M. C. Payne, *Z. Kristallogr.* **2005**, *220*, 567.
[35] J. P. Perdew; A. Zunger, *Phys. Rev. B* **1981**, *23*, 5048.
[36] F. Ortmann; F. Bechstedt; W. G. Schmidt, *Phys. Rev. B* **2006**, *73*, 205101.
[37] C. Bonhomme; C. Gervais; F. Babonneau; C. Coelho; F. Pourpoint; T. Azaïs; S. E. Ashbrook; J. M. Griffin; J. R. Yates; F. Mauri; C. J. Pickard, *Chem. Rev.* **2012**, *112*, 5733.
[38] S. Baroni; S. Gironcoli; A. D. Corso; P. Giannozzi, *Rev. Mod. Phys.* **2001**, *73*, 515.
[39] G. R. Qian; X. Dong; X.-F. Zhou; Y. Tian; A. R. Oganov; H.-T. Wang, *Comput. Phys. Commun.* **2013**, *184*, 2111.
[40] G. Kresse; J. Furthmüller, *Phys. Rev. B* **1996**, *54*, 11169.
[41] C. W. Glass; A. R. Oganov; N. Hansen, *Comput. Phys. Commun.* **2006**, *175*, 713.

Manuscript received: May 16, 2025
Revised manuscript received: June 9, 2025
Version of record online: ■■, ■■

RESEARCH ARTICLE

Carbon nanothread (CNTh) is a family of 1D diamond-like materials, which was predicted to have extremely high strength, stiffness, and tenacity, but suffered from its disordered intrathread bonding. By a nonsymmetric F-substitution on benzene, we synthesized atom-scale ordered CNTh with specific structure out of many isomeric competitors. Our work paved the way to the precise construction of diamond-like material.

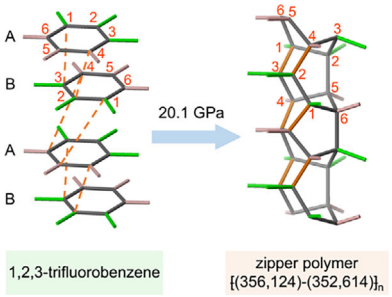

G. Che, X. Tang, P. Lang, J. Liu, Y. Wang, X. Wang, X. Wang, J. Ju, A. Guan, Q. Li, J. Xiang, L. Guo, Y. Qiao, X. Dong, H.-kwang Mao, H. Zheng, K. Li

1 – 8

Fluorine-Directed Structure-Specific Carbon Nanothreads